Chemosphere 283 (2021) 131199

Contents lists available at ScienceDirect

Chemosphere

journal homepage: www.elsevier.com/locate/chemosphere

Transformation of short-chain chlorinated paraffins and olefins with the bacterial dehalogenase LinB from *Sphingobium Indicum* – Kinetic models for the homologue-specific conversion of reactive and persistent material

Marco C. Knobloch [a,b,*], Lena Schinkel [a,c], Hans-Peter E. Kohler [c], Flurin Mathis [d], Susanne Kern [d], Davide Bleiner [a,b], Norbert V. Heeb [a]

[a] *Laboratory for Advanced Analytical Technologies, Swiss Federal Institute for Materials Science and Technology Empa, Überlandstrasse 129, 8600, Dübendorf, Switzerland*
[b] *Department of Chemistry, University of Zürich, Winterthurerstrasse 190, 8057, Zürich, Switzerland*
[c] *Swiss Federal Institute of Aquatic Research and Technology Eawag, Überlandstrasse 129, 8600, Dübendorf, Switzerland*
[d] *Zürich University of Applied Sciences ZHAW, Unterstrass 31, 8820, Wädenswil, Switzerland*

ARTICLE INFO

Handling Editor: Derek Muir

Keywords:
Chlorinated olefins (COs)
Chlorinated paraffins (CPs)
Enzymatic dechlorination
First-order kinetic model
Persistent organic pollutants (POPs)

ABSTRACT

Structure, reactivity and physico-chemical properties of polyhalogenated compounds determine their uptake, transport, bio-accumulation, transformation and toxicity and their environmental fate. In technical mixtures of chlorinated paraffins (CPs), these properties are distributed due to the presence of thousands of homologues. We hypothesized that roles of CP dehalogenation reactions, catalyzed by the haloalkane dehalogenase LinB, depend on structural properties of the substrates, e.g. chlorination degree and carbon-chain length. We exposed mixtures of chlorinated undecanes, dodecanes and tridecanes *in-vitro* to LinB from *Sphingobium Indicum* bacteria. These single-chain CP-materials also contain small amounts of chlorinated olefins (COs), which can be distinct by mathematical deconvolution of respective mass-spectra. With this procedure, we obtained homologue-specific transformation kinetics of substrates differing in saturation degree, chlorination degree and carbon chain-length. For all homologues, two-stage first-order kinetic models were established, which described the faster conversion of reactive material and the slower transformation of more persistent material. Half-lifes of 0.5–3.2 h and 56–162 h were determined for more reactive and more persistent CP-material. Proportions of persistent material increased steadily from 18 to 67% for lower (Cl_6) to higher (Cl_{11}) chlorinated paraffins and olefins. Conversion efficiencies decreased with increasing chlorination degree from 97 to 70%. Carbon-chain length had only minor effects on transformation rates. Hence, the conversion was faster and more efficient for lower-chlorinated material, and slower for higher-chlorinated and longer-chained CPs and COs. Current legislation has banned short-chain chlorinated paraffins (SCCPs) and forced a transition to longer-chain CPs. This may be counterproductive with regard to enzymatic transformation with LinB.

1. Introduction

Chlorinated paraffins (CPs) with carbon chain-lengths of C_{10} to C_{30} and chlorine contents of 30–70% (m/m) are produced by radical chlorination of respective *n*-alkanes (Fiedler, 2010; Glüge et al., 2016). More than one million tons CPs are produced yearly (Glüge et al., 2016; van Mourik et al., 2016). CPs are used as flame retardants and plasticizers in plastic materials, as metal working fluids, and as additives in paints (Muir et al., 2000; UNEP, 2012; Glüge et al., 2016). Technical CPs are complex mixtures of thousands of isomers with variable chain-length and chlorination degree (Tomy, 2010; Sprengel and Vetter, 2020; Yuan et al., 2020). CPs are commonly classified as short-(SCCPs, C_{10}–C_{13}), medium- (MCCPs, C_{14}–C_{17}), long- (LCCPs, C_{18}–C_{21}) and very long- (vLCCPs, C_{22}–C_{30}) CPs (Diefenbacher et al., 2015; UNEP, 2016). SCCPs show persistent, bioaccumulating and toxic properties and the potential for long-range transport (Iozza et al., 2009a; Vorkamp and Rigét, 2014; Labadie et al., 2019; Wang et al., 2019). In 2017, SCCP have been listed as persistent organic pollutants (POPs) under the Stockholm

* Corresponding author. Laboratory for Advanced Analytical Technologies, Swiss Federal Institute for Materials Science and Technology Empa, Überlandstrasse 129, 8600, Dübendorf, Switzerland.
E-mail address: marco.knobloch@empa.ch (M.C. Knobloch).

https://doi.org/10.1016/j.chemosphere.2021.131199
Received 26 March 2021; Received in revised form 12 May 2021; Accepted 9 June 2021
Available online 14 June 2021

Convention (UNEP, 2017). MCCPs are currently under evaluation for EU-wide restrictions (ECHA, 2019; de Wit et al., 2020). Environmental and metabolic transformation pathways of CPs are widely unknown. Considering the amounts produced and wide applications of CPs, their environmental and metabolic fate and toxicity needs further investigations.

1.1. Challenging analysis of CPs and their transformation products

Currently, monitoring CPs in environmental samples requires a chromatographic method coupled to a mass analyzer (van Mourik et al., 2018; Krätschmer and Schächtele, 2019). Chromatographic separation of CPs is only partially achieved (Iozza et al., 2009b; Perkons et al., 2019; Matsukami et al., 2020). Therefore, mass analyzers must provide sufficient mass resolution (e.g. R ≈ 120′000) to resolve interferences of different CP homologues and chlorinated olefins (COs), which are CP transformation products (Schinkel et al., 2018a; Mézière et al., 2020). In this manuscript the term material is used to denote mixtures of CPs and COs. For example, chloroundecane material denotes a mixture of chloroundecanes and chloroundecenes.

To reduce CP-CP interferences, single-chain materials can be used as substrates for transformation studies (Schinkel et al., 2018b; Sprengel et al., 2019; Heeb et al., 2020).

The presence of CP transformation products can lead to additional interferences. For example, exposure of CPs to heat and reactive metal surfaces facilitates elimination of hydrogen chloride (HCl) of CPs to unsaturated compounds such as chlorinated olefins (COs) and di-olefins (CdiOs) (Schinkel et al., 2018a). Isotope clusters of paraffinic, olefinic and di-olefinic material interfere (Schinkel et al., 2017; Knobloch et al., 2021). We developed a mathematical deconvolution procedure, which was used to obtain non-interfered CP-, CO- and CdiO- data (Schinkel et al., 2017; Knobloch et al., 2021). Hydroxylated CP-transformation products have been identified recently, which may interefere with CPs (Chen et al., 2020; He et al., 2020; Knobloch et al., 2021).

1.2. Dehalogenation reactions of CPs

CPs are considered as chemically stabile molecules. However, some transformation reactions of CPs have been observed (Liu et al., 2015; Schinkel et al., 2018b; Chen et al., 2020). CPs can be transformed by breaking carbon-chlorine bonds (Lal and Saxena, 1982). Fig. 1 displays three types of dechlorination reactions which may be catalyzed by different dehalogenation enzymes (Vogel et al., 1987; Belkin, 1992; Faber, 2018).

Reductive dehalogenation reactions (Fig. 1A, Cl → H) of CPs and, if present, COs lead to products with lower chlorination degrees. Thus, most of the formed products during reductive dechlorination are already present in the starting material. Indications were found that reductive dehalogenation processes of CPs can occur in rice cells and pumpkin seedlings (Li et al., 2019; Chen et al., 2020).

CPs can undergo abiotic HCl elimination reactions (Fig. 1B) (Bergman et al., 1984; Schinkel et al., 2018a). These reactions are catalyzed by dehydrohalogenases like the LinA-enzyme of certain *Sphingobium* species, converting chlorinated paraffins to less chlorinated olefins (Fig. 1B) (Heeb et al., 2019). Because mass spectra of paraffinic and olefinic strongly overlap, monitoring of such elimination reactions is challenging (Schinkel et al., 2017, 2018b, 2018b).

Dehalohydroxylation reactions of CPs results in dechlorinated alcohols (Cl → OH, Fig. 1C). The haloalkane dehalogenase LinB, also expressed in certain *Sphingobium* species, catalyzes the hydrolysis of halogenated compounds (Nagata et al., 1999; Lal et al., 2010; Heeb et al., 2012, 2013) to hydroxylated products with lower halogenation degree (Fig. 1C). We could show that LinB also catalyzes the transformation of chlorinated tridecanes (C_{13}-CPs) to hydroxylated metabolites (Knobloch et al., 2021).

CPs are complex mixtures of thousands of isomers (Tomy, 2010; Yuan et al., 2020). Therefore, it is likely that certain CP isomers are suitable substances for enzymatic transformations while others are not converted and persist. Carbon chain-length, chlorination degree and stereochemistry might affect biotransformation. The question comes up, which CP- and CO-homologues are metabolized and which persist.

1.3. Study objectives

We performed a study to investigate effects of chlorination degrees and chain length on the transformation of CPs and COs by the dehalohydroxylase LinB. We could show that SCCPs are converted to mono- and di-hydroxylated transformation products under LinB-exposure (Knobloch et al., 2021). Herein we focus only on the CP and CO conversion.

We exposed single-chain SCCP materials with carbon-chain lengths of C_{11}, C_{12} and C_{13} to the dehalogenase LinB from *Sphingobium indicum*. Interfered isotope clusters of paraffinic and olefinic material were resolved with mathematical deconvolution. A bimodal first-order kinetic model was applied to model homologue specific dechlorination kinetics for CPs and COs. This comparative kinetic study allows an assessment of reactivity and persistence of different CP homologues. Thus, it may influence alternative regulations for technical CP mixtures, which may also depend on the chlorination degree of CPs rather than on the carbon chain-length.

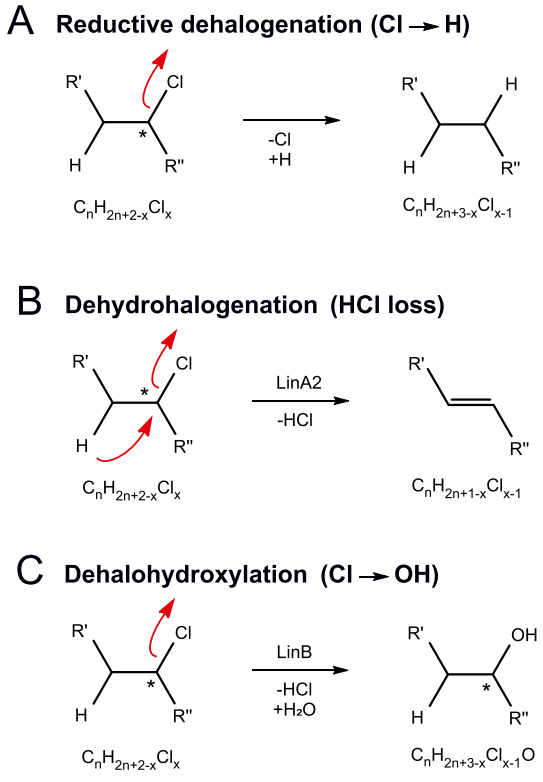

Fig. 1. Possible enzymatic dechlorination reactions of chlorinated paraffins (CPs) and olefins (COs). Chiral centers are marked with asterix (*). In reductive dehalogenation reactions (A), chlorine is replaced by hydrogen resulting in products with lower chlorination degree. Dehydrohalogenation reactions (B) transform CPs into COs and COs into chlorinated diolefins (CdiOs) by elimination of HCl. Dehalohydroxylation reactions (C) convert CPs and COs in respective alcohols. Nucleophilic substitution of chlorides with a hydroxy group can occur with (S_N2) and without (S_N1) stereoinversion. Respective transformation products have lower chlorination degrees and are more polar. Similar transformation reactions may happen under abiotic conditions. Some of these transformation products can already be present in the starting material.

2. Experimental section

2.1. Chemicals, substrates, and enzyme

Mixtures of chloroundecanes (m_{Cl} = 65.25%), chlorododecanes (m_{Cl} = 65.08%) and chlorotridecanes (m_{Cl} = 65.18%) obtained from Dr. Ehrenstorfer (Augsburg, Germany) were used as substrates. δ-HBCD (Empa, Dübendorf, Switzerland) was used as internal standard (IS). Methanol, ethyl acetate, dichloromethane (all from Biosolve, Valkenswaard, Netherlands), purified water (Milli-Q Reference A+, 18.2 MΩcm) and acetone (Merck, Darmstadt, Germany) were used as solvents. Glycine and tris(hydroxymethyl)amino methane (tris) (Sigma-Aldrich, Buchs, Switzerland) were used as buffer materials. The LinB enzyme from *Sphingobium Indicum* was obtained through heterologous expression from *Escherichia coli* as described elsewhere (Knobloch et al., 2021).

2.2. Enzymatic incubation and LC-MS analysis

1000 μL of each SCCP-mixture (10 ng/μL) in cyclohexane was transferred to brown glass vials and concentrated to dryness by an N_2 stream. Residues were dissolved in acetone (500 μL), mixed with buffer (364 mM glycine, 50 mM tris, pH 8.3, 2500 μl) and diluted with water (1714 μl). After withdrawing two control samples (471 μL), LinB solution (229 μL, 1.75 μg/μL, 400 μg) was added. Concentration of CPs (2 ng/μL), LinB-enzyme (100 ng/μL), acetone (10 vol%), tris (25 mM) and glycine (182 mM) are expected. One sample was prepared for each chloroundecanes, chlorododecanes and chlorotridecanes. Samples were incubated at room temperature and shaken at 100 rounds per minute. After 2, 4, 8, 24, 48, 72 and 144 h, aliquots (500 μL) were taken for analysis. Immediately after collecting the samples, ethyl acetate (500 μL) was added. IS (δ-HBCD, 50 ng) was added and samples were stored at −20 °C. Aqueous phases were extracted with ethyl acetate (3 × 500 μL). Organic supernatant was removed, combined and reduced to dryness by an N_2 stream. Residues were dissolved with 100 μL methanol. Control samples, exposed to buffer and acetone only, were treated analogously. Control samples were taken at start (t = 0 h) and after 144 h. Samples were analyzed twice with a liquid chromatography time-of-flight mass spectrometer with an atmospheric pressure chemical ionization source (LC-APCI-QTOF-MS), which favors a formation of chloride-adducts ions $[M+Cl]^-$ of CPs. This method is described in detail elsewhere (Knobloch et al., 2021).

2.3. Mathematical deconvolution of interfered mass spectra

Isotope clusters in mass spectra of chlorinated paraffinic (CPs), mono-olefinic (COs) and diolefinic (CdiOs) substances interfere at the applied mass resolution of R ≈ 8000 (Schinkel et al., 2018a; Knobloch et al., 2021). A mathematical deconvolution procedure was used to obtain non-interfered isotope clusters and signal-intensities of CPs, COs and CdiOs from interfered mass spectra. The deconvolution procedure relies on linear combination of calculated isotope cluster and is presented elsewhere (Yuan et al., 2016; Schinkel et al., 2017, 2018b, 2018b; Heeb et al., 2020). The workflow of the procedure is briefly described in the supporting information (Figure S1). Expected isotope clusters of chloride-adducts of hexa-to undecachlorinated C_{11}-, C_{12}- and C_{13}-CPs, -COs and -CdiOs were calculated with EnviPat (Loos et al., 2015) and are given in Tables S1–S9. Mathematical deconvolution also delivers proportions (%) of paraffinic (p_{CP}), mono-olefinic (p_{CO}) and di-olefinic (p_{CdiO}) material. In addition, signal intensities (cts) of interfering isotope cluster are obtained. The signal intensities are corrected with theoretical abundance and total signal intensities $I_{100\%}$ for CPs ($I_{CP,100\%}$), COs ($I_{CO,100\%}$) and CdiOs ($I_{CdiO,100\%}$) are deduced (Tables S10–S12). These data are used to model transformation kinetics and to calculate chlorination degrees as mean chlorine-number (n_{Cl}) and as chlorine mass percentage (m_{Cl}).

2.4. Data extraction, background subtraction, kinetic model

Data evaluation was done with MassHunter Qualitative Analysis B.07.00 (Agilent, Santa Clara CA, USA). Mean mass spectra were obtained by extracting respective chromatographic peaks with the MassHunter software. To reduce noise levels, background mass spectra of blank samples was subtracted from original mass spectra. Background spectra were obtained by extracting mean spectra in the retention range in which CPs, COs and CdiOs elute. The effect of background subtraction on a measured isotope clusters is shown in Figure S2. Background subtracted isotope clusters show less noise and produce more reliable deconvolution models compared to non-corrected ones.

2.5. Kinetic modelling

A bimodal first-order kinetic model, which was introduced to model CP transformation with the LinA2-enzyme (Heeb et al., 2019), was also applied for LinB-kinetics. The bimodal first-order kinetic model was applied to non-interfered signal intensities in relation to values at start ($I_{t,100\%}/I_{0,100\%}$). The algorithm *lsqcurvefit* in MATLAB R2018a (MathWorks, Natick USA) was used to fit mathematical models to experimental data. Figure S4 shows modeled bimodal first-order kinetics for reactive and persistent material on the example of $C_{13}Cl_8$-CPs. For all exposed CP- and CO-homologues, a fast transformation within the first 8 h and a slower conversion in a latter phase was observed, as discussed below (chapter 3.3). Half-live values of homologues converted in the faster first phase and the slower latter phase were deduced from these models. In this manuscript, materials with half-live values in order of hours are referred to as reactive and of days as persistent.

The reaction rates of the persistent CP and CO-homologues were modeled with a first-order reaction kinetics according to equation (1) from data points in the slower phase (t ≥ 8 h). The model delivers the proportion (p_p) and reaction constant (k_p) of persistent material.

$$\ln\left(\boldsymbol{I}_{\boldsymbol{t,p},\ 100\%} \,/\, \boldsymbol{I}_{0,\ 100\%}\right) = \ln\left(\boldsymbol{p}_{\boldsymbol{p}}\right) - \boldsymbol{k}_{\boldsymbol{p}}{}^{*}\boldsymbol{t} \tag{1}$$

Proportion of reactive material (p_r) is obtained from $\boldsymbol{p}_{\boldsymbol{r}} = 1 - \boldsymbol{p}_{\boldsymbol{p}}$. Equation (2) shows the first-order kinetics of reactive material.

$$\ln\left(\boldsymbol{I}_{\boldsymbol{t,r},\ 100\%} \,/\, \boldsymbol{I}_{0,\ 100\%}\right) = \ln\left(\boldsymbol{p}_{\boldsymbol{r}}\right) - \boldsymbol{k}_{\boldsymbol{r}}{}^{*}\boldsymbol{t} \tag{2}$$

The kinetics for persistent (equation (1)) and reactive (equation (2)) material are composed together, resulting in equation (3). Reaction constant of the reactive material (k_r) is received by fitting all data points in the faster phase according to equation (3).

$$I_{t,\ 100\%} \,/\, I_{0,\ 100\%} = p_r \cdot e^{-k_r{}^{*}t} + p_p \cdot e^{-k_p{}^{*}t} \tag{3}$$

First-order rate constants for persistent (k_p) and reactive (k_r) material were used to deduce half-life values ($t_{1/2,\ p}$, $t_{1/2,\ r}$) according to equation (4).

$$\boldsymbol{t}_{1/2} = \ln(2)/\boldsymbol{k} \tag{4}$$

with the applied bimodal kinetic model, we obtained first-order rate constants (k_p, k_r), half-life values ($t_{1/2,\ p}$, $t_{1/2,\ r}$), and proportions (p_p, p_r) of reactive and persistent CPs and COs homologues (Table S13).

We applied the model to all measured data points and did not exclude potential outliers. As discussed on the example of C_{12}-CPs in SI (chapter S1.3), observed trends deduced from the models do not differ substantially if data are excluded from the model (Table S14).

3. Results and discussion

3.1. Comparison of non-exposed and LinB-exposed CP mass spectra

Mass spectra of non-exposed and LinB-exposed (144 h) chloroundecanes (C_{11}, A, B), chlorododecanes (C_{12}, C, D) and

chlorotridecanes (C_{13}, E, F) are given in Fig. 2. Chloride-adduct ions $[M+Cl]^-$ are observed under the given conditions due to enhanced chloride formation in the APCI source of the instrument.

Hexa-to deca-chlorinated homologues were detected in the C_{11}-materials and $C_{11}Cl_8$-homologues were most abundant (Fig. 2 A). Hexa-to undeca-chlorinated homologues were found in C_{12}- and C_{13}-materials (Fig. 2 C, E). Most prominent were $C_{12}Cl_9$-and $C_{13}Cl_9$-homologues (Fig. 2 C, E). The $C_{11}Cl_8$-, $C_{12}Cl_9$-and $C_{13}Cl_9$-homologues remained most abundant in respective LinB-exposed mixtures (Fig. 2 B, D, F). As indicated by dashed lines, small changes of homologue distributions were observed in all cases after exposure to LinB (Fig. 2). Some $C_{11}Cl_6$-and $C_{12}Cl_6$-homologues were detected before exposure (Fig. 2 A, C) but not anymore after LinB-exposure (144 h) (Fig. 2 B, D). As a general trend, proportions of lower-chlorinated Cl_6-and Cl_7-homologues decreased during enzymatic exposure, while those of higher-chlorinated Cl_9-, Cl_{10}- and Cl_{11}-homologues increased to some degree.

Measured isotope clusters are interfered and both, paraffinic and olefinic materials could be found. Mathematical deconvolution delivered non-interfered isotope clusters and proportions of chlorinated paraffins (p_{CP}), olefins (p_{CO}) and diolefins (p_{CdiO}). Fig. 3 compares measured and modeled isotope clusters of non-exposed chloroundecane material. In this example, paraffin proportions (p_{CP}) of hexa-, hepta-, octa-, nona- and deca-chloroundecanes of 60, 82, 91, 95 and 98% were determined. Respective olefin proportion (p_{CO}) were 26, 25, 9, 5 and 2% as indicated in Fig. 3. Paraffin- and olefin- and, if present, diolefin-proportions of non-exposed, LinB-exposed, and control samples are reported in Tables S10–S12, together with non-interfered signal intensities $I_{100\%}$ of CPs, COs and CdiOs.

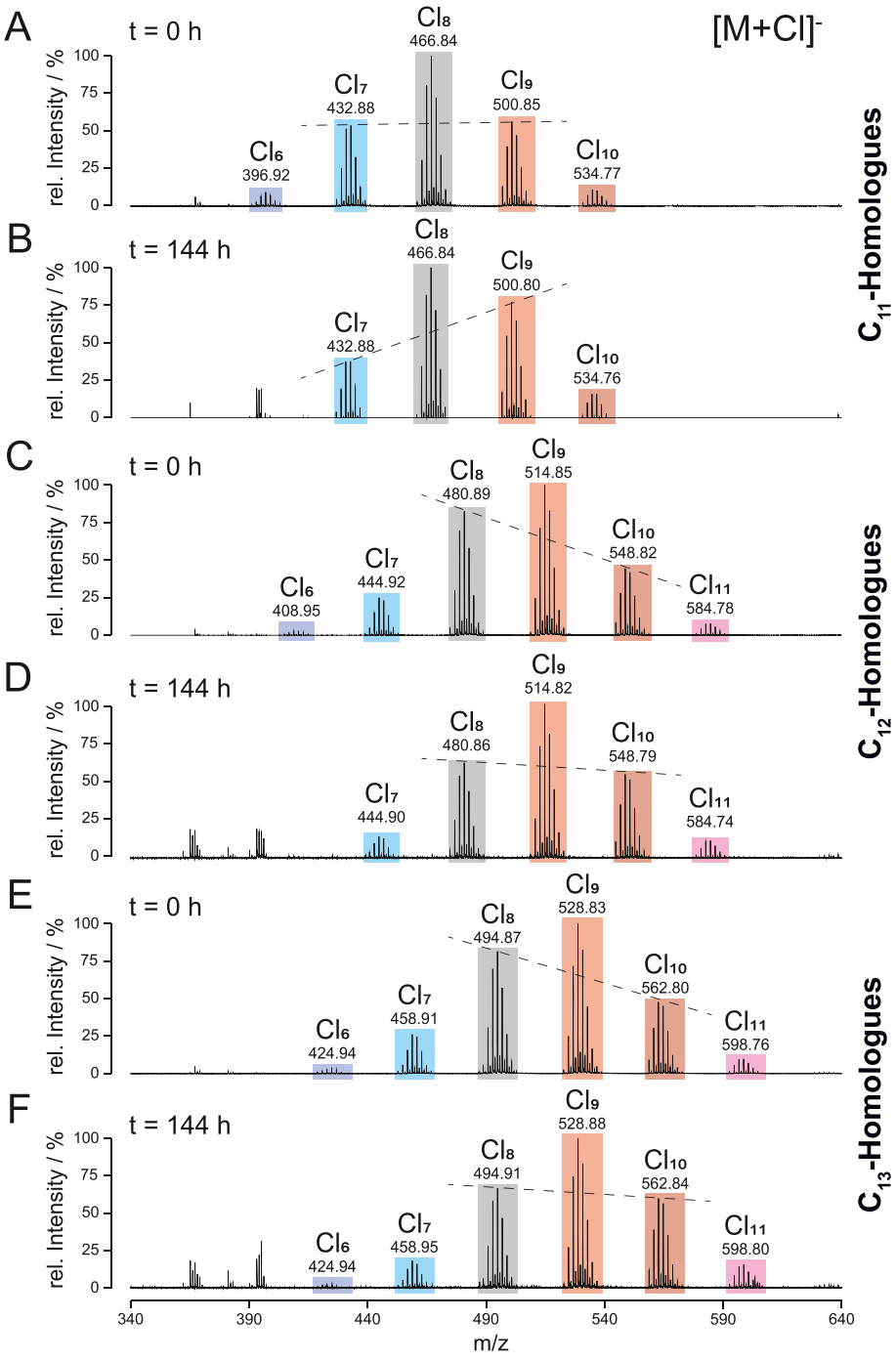

Fig. 2. Normalized APCI-QTOF-mass spectra (R ≈ 8′000) of non-exposed and LinB-exposed (144 h) materials. Under the given MS conditions $[M+Cl]^-$-adduct ions are formed for CPs and COs. Spectra of non-exposed and LinB-exposed C_{11}- (A,B), C_{12}- (C,D) and C_{13}- (E,F)-homologues are compared. Hexa- (Cl_6, dark blue), hepta- (Cl_7, blue), octa- (Cl_8, gray), nona- (Cl_9, red), deca- (Cl_{10}, dark red) and undeca-(Cl_{11}, magenta) chlorinated compounds are distinguished. Changes of homologue distributions (dashed lines) can be observed by comparing spectra of non-exposed (A, C, E) and LinB-exposed (B, D, F) materials. (For interpretation of the references to colour in this figure legend, the reader is referred to the Web version of this article.)

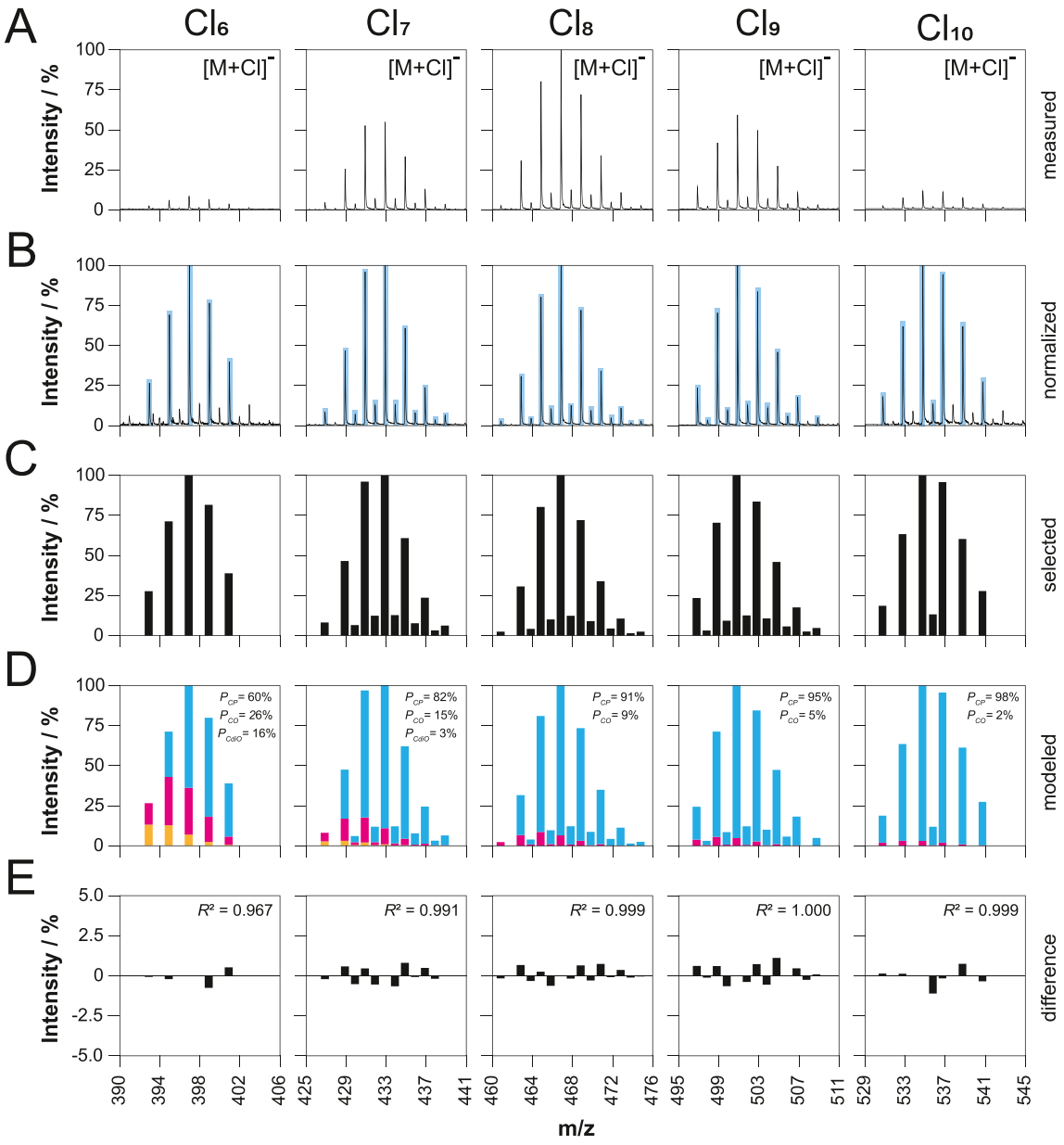

Fig. 3. Mathematical deconvolution of interfered mass spectra of non-exposed C11-CPs and -COs. Under the given APCI-MS conditions chloride adducts [M+Cl]- are observed. Measured (A) and normalized (B) isotope clusters of hexa-to deca-chlorinated materials were extracted from the mass spectrum. Ions selected for deconvolution are given (C). Paraffinic (blue), olefinic (magenta) and in some cases diolefinic (orange) materials are distinguished (D). Proportions of chlorinated paraffins (p_{CP}) increased from 60% to 98%, while respective proportions of chlorinated olefins (p_{CO}) decreased from 26% to 2% for hexa-to decachlorinated compounds. Differences of measured and modeled isotope clusters are small (<2%) in all cases (E). (For interpretation of the references to colour in this figure legend, the reader is referred to the Web version of this article.)

A comparison of measured and deconvoluted isotope clusters of the starting materials and control samples that were exposed for 144 h to buffer only (Figure S4), does not indicate any changes of homologue distributions. Because exposure to buffer alone did not induce dechlorination reactions. We conclude that observed effects on homologue distribution in LinB-exposed samples were enzyme-catalyzed.

3.2. *Enzyme-catalyzed dechlorination of CPs and COs*

Deconvolution of isotope clusters of major homologues, which were exposed to LinB for 0, 2, 24 and 144 h revealed small changes in CP- and CO-proportions. Figure S5 compares CP- and CO-changes observed for C_{11}-, C_{12}- and C_{13}-materials. In non-exposed materials, CP-proportions p_{CP} increase with increasing degree of chlorination from 60 to 95% for Cl_6-to Cl_{10}-homologues, while proportions of chlorinated olefins p_{CO} (calculated as sum of mono- and di-olefins) decrease from 40 to 5%. Paraffin proportions decreased for each homologue class during prolonged enzyme exposure by about 1–20%. Accordingly, olefin proportions increased, as indicated by dashed lines in Figure S5. In other words, olefinic material is more persistent towards LinB conversion than paraffinic material. Effects were more pronounced for lower chlorinated Cl_6-and Cl_7-homologues.

HCl-Elimination reactions of paraffinic materials (Fig. 1B) would lead to lower-chlorinated olefins. This would be in accordance with the observed trends. However, such elimination reactions of Cl_6-CPs should deliver $C_{11}Cl_5$-, $C_{12}Cl_5$-and $C_{13}Cl_5$-chloroolfefins. But typical isotope clusters of these substances were not observed after LinB-exposure. We conclude that elimination reactions are not induced by LinB. But olefinic

proportions rise with respect to paraffins, because olefins are less reactive towards LinB-transformations than paraffins. Therefore, COs accumulated in relative amounts to paraffins in the remaining material.

Fig. 4 shows chlorination degrees n_{Cl} of C_{11}- (A), C_{12}- (B) and C_{13}- (C) CPs and COs together with distributions of hexa-to undeca-chlorinated homologues during LinB-exposure (0–144 h). Chlorine numbers (n_{Cl}) of respective samples are given in Table S15. CP- and CO-distributions show that proportions of lower-chlorinated homologues (Cl_6, Cl_7 and Cl_8) decrease, while proportions of higher-chlorinated homologues (Cl_9, Cl_{10}) increase during LinB-exposure (Fig. 4). An increase of chlorine number n_{Cl} during LinB-exposure is observed for all CP and CO materials. Chlorination degrees of C_{11}-, C_{12}- and C_{13}-CPs increased during LinB-exposure (144 h) from 8.11 to 8.38 ($\Delta n_{Cl} = 0.27$), from 8.84 to 9.07 ($\Delta n_{Cl} = 0.23$), and from 8.86 to 9.09 ($\Delta n_{Cl} = 0.23$), respectively. At start, chlorination degrees of C_{11}-, C_{12}- and C_{13}–COs were generally lower than those of respective CPs (Δn_{Cl} = 0.50, 0.57 and 0.49). However, during LinB-exposure, C_{11}-, C_{12}- and C_{13}–CO chlorination degrees also increased from 7.61 to 7.91 (Δn_{Cl} = 0.30), from 8.27 to 8.55 (Δn_{Cl} = 0.28), and from 8.37 to 8.61 (Δn_{Cl} = 0.24), respectively. Observed increase of the chlorination degrees of CPs and COs after 144 h (Δn_{Cl}) are 1.7–23.0 times higher than the standard deviation of the chlorination degrees (Table S15). All three starting materials show an increase of the CP and CO chlorination degree during exposure to LinB.

Therefore, we conclude that higher-chlorinated CP and CO homologues are more persisting against LinB-catalyzed transformation and higher-chlorinated materials accumulated in relative amounts during LinB-exposure. This would shift the homologue distribution to higher chlorinated homologues. A study with pumpkin seedlings shows that higher chlorinated CPs accumulated in biological system more than lower chlorinated ones (Li et al., 2019). Together with our results, this may show that the chlorination degree is a relevant factor to be included in the environmental and toxicological risk assessment.

3.3. *Homologue-specific transformation kinetics of persistent and reactive CPs with LinB*

Fig. 5 displays non-interfered relative signal intensity data ($I_{t,100\%}/I_{0,100\%}$) of hexa- (Cl_6) to undeca- (Cl_{11}) chlorinated undecanes (C_{11}, A), dodecanes (C_{12}, B) and tridecanes (C_{13}, C) during LinB-exposure (0–144 h). A bimodal first-order model was applied to all measured data points and we did not exclude potential outliers. For all CP-homologues, conversion is fast in a first phase (≤8 h) and slow in a second phase (≥8 h). From these trends, we conclude that both, reactive and more persisting materials are present in each CP homologue class. These trends were observed in all three independent samples. Enzyme activity may be decreased during prolonged exposure time, which may influence the conversion rate of CPs and COs. One would expect a linear decrease of the enzyme activity, but we observed an abrupt change from faster to slower conversion rates at 8 h in the three independent experiments. Therefore, we conclude that the presence of reactive and persistent homologues lead to a bimodal LinB-catalyzed conversion course.

The applied kinetic model describes conversions of both fractions with first-order kinetics. The same observation, the fast conversion of reactive CP material in the early phase and the slower conversion of

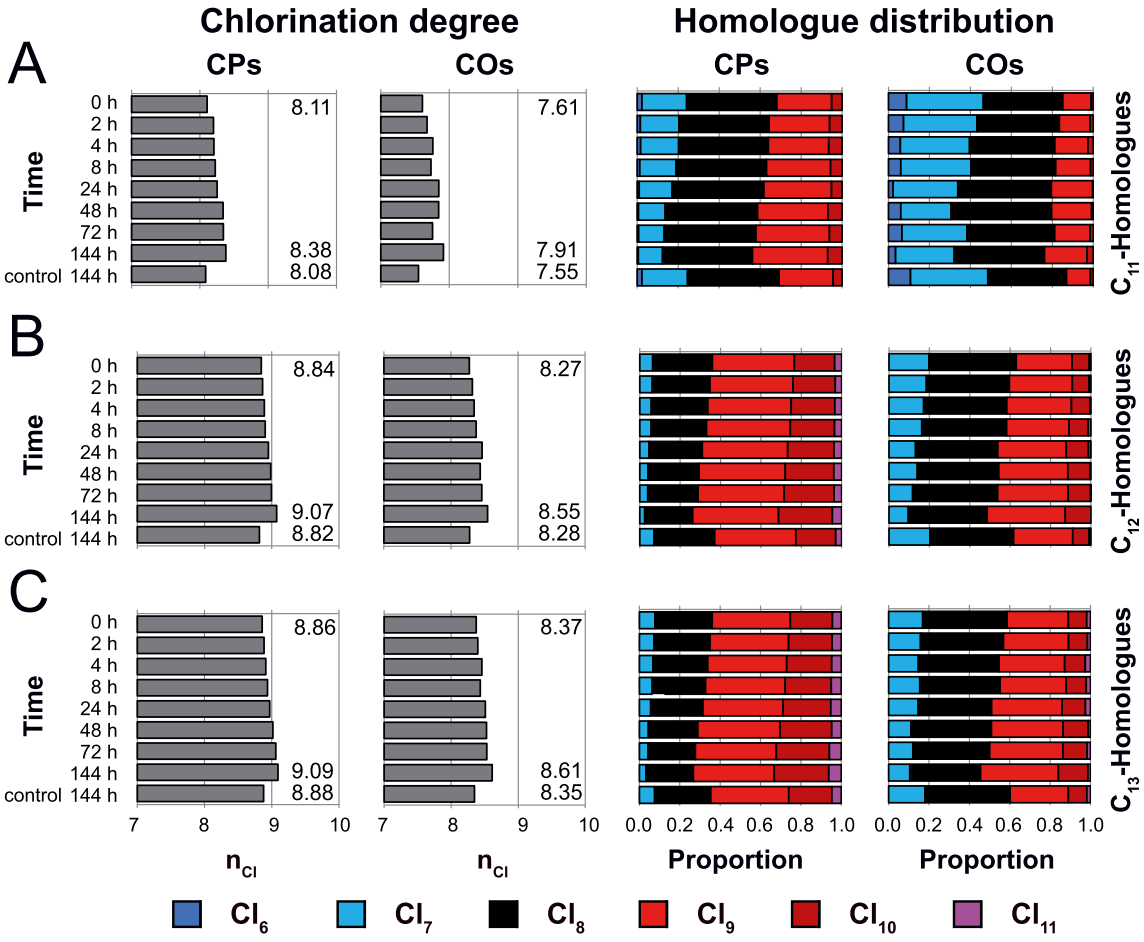

Fig. 4. Chlorination degrees (n_{Cl}) and changes of homologue distributions in chlorinated paraffins and olefins during LinB exposure. Proportions of hexa- (blue), hepta- (light blue), octa- (black), nona- (red), deca- (dark red) and undeca- (magenta) chlorinated C_{11}- (A), C_{12}- (B), and C_{13}- (C) homologues are shown for non-exposed (0 h), LinB-exposed (2–144 h) and buffer-exposed (control, 144 h) samples. (For interpretation of the references to colour in this figure legend, the reader is referred to the Web version of this article.)

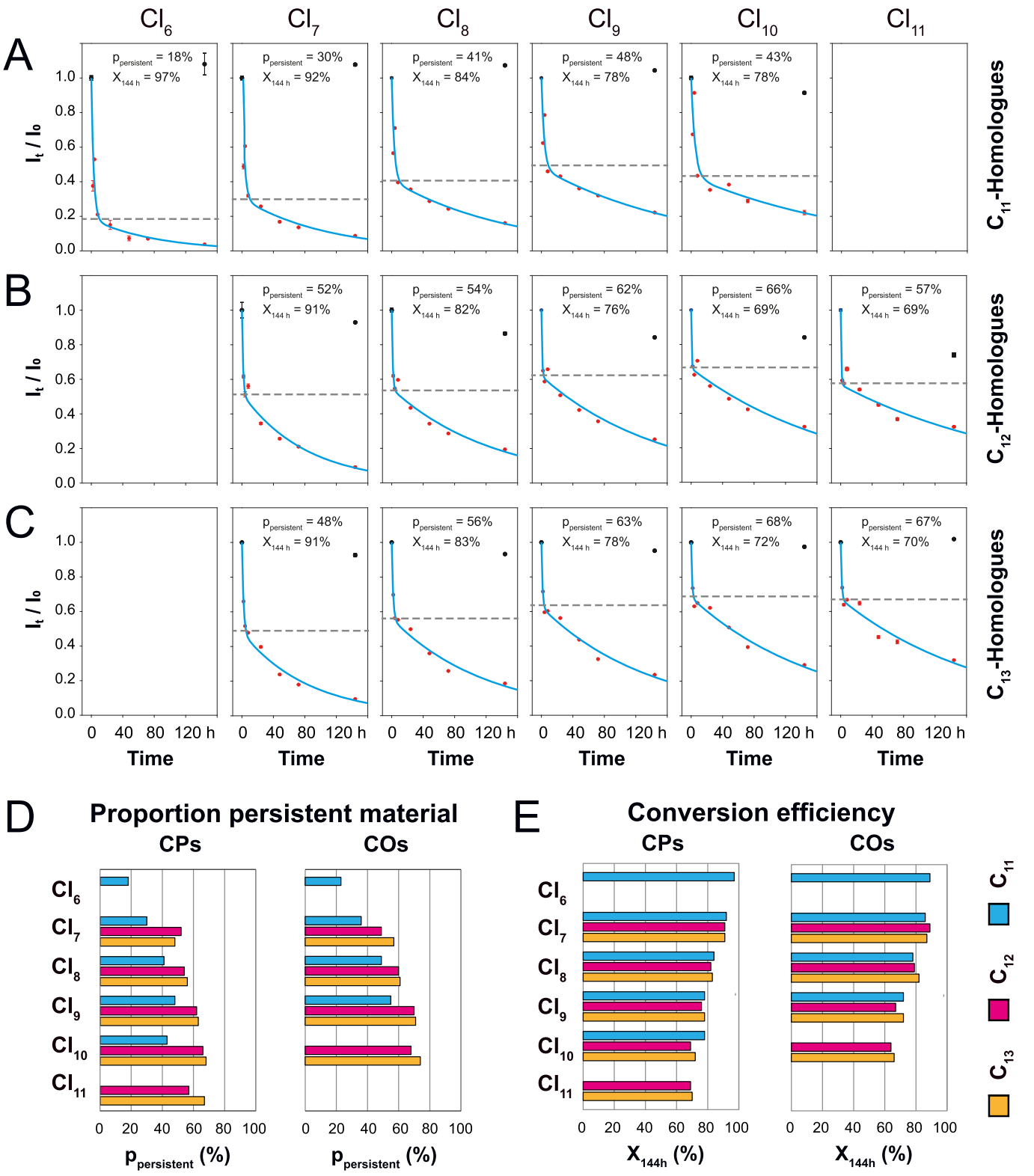

Fig. 5. Homologue-specific, bimodal first-order kinetics (A–C) of CPs during LinB exposure. Relative signal intensities (I_t/I_0) of non-exposed (black, 0 h), LinB-exposed (red, 2–144 h) and buffer-exposed samples (control, black, 144 h) are depicted for Cl_6-to Cl_{11}-undecanes (A), -dodecanes (B) and -tridecanes (C). Respective bimodal kinetic models (blue lines) for the conversion of persistent and reactive materials are shown. Reactive material is quickly converted within ≤8 h, more persistent material is transformed slower in a second phase. Proportions (p_p) of more persistent CP- and CO-material were deduced from the bimodal kinetic model (D). Respective values are indicated (gray dotted lines, A-C). Calculated total conversions X_{144h} after 144 h is also given for CPs and COs (E). C_{11}- (light blue), C_{12}- (magenta) and C_{13}- (orange) homologues are distinguished (D, E). (For interpretation of the references to colour in this figure legend, the reader is referred to the Web version of this article.)

more persistent CPs in the latter phase, was made on the conversion of SCCPs with the LinA2-enzyme (Heeb et al., 2019) and is compared with the results on LinB-conversion below in chapter 3.5.

As shown in Fig. 5, modeled (blue lines) and measured (red dots) data are in good agreement for all CP-homologues. The kinetic model allows to deduce proportions of reactive (p_r) and persistent (p_p) materials, which are indicated as dashed lines in Fig. 5. Table S13 lists proportions of persistent materials p_p and total conversion efficiencies X_{144h} after 144 h LinB-exposure.

Fig. 5D compares total conversion efficiencies (X_{144h}) of CPs and COs and proportions of persistent materials (p_p) of C_{11}- (blue), C_{12}- (magenta) and C_{13}- (orange) CPs and COs. Conversion efficiencies decreased with increasing chlorination number. On average, efficiencies of 97%, 91%, 83%, 78%, 77% and 70% were obtained for Cl_6-, Cl_7-, Cl_8-, Cl_9-, Cl_{10}-, and Cl_{11}-homologues, respectively. Carbon-chain length had no significant effect on the conversion efficiency, but the effect of the chlorination degree was substantial.

Proportions of persistent material (Fig. 5D) for chloroundecanes (blue) are generally lower than for chlorododecanes (magenta) and chlorotridecanes (orange). Proportions of persistent material on average increased with higher chlorination degree from 18%, 43%, 50%, 58%, 59%, and 62% for Cl_6-, Cl_7-, Cl_8-, Cl_9-, Cl_{10}-, and Cl_{11}-homologues, respectively. We conclude that the chlorination degree has significant effects both, on the overall conversion efficiency and proportion of

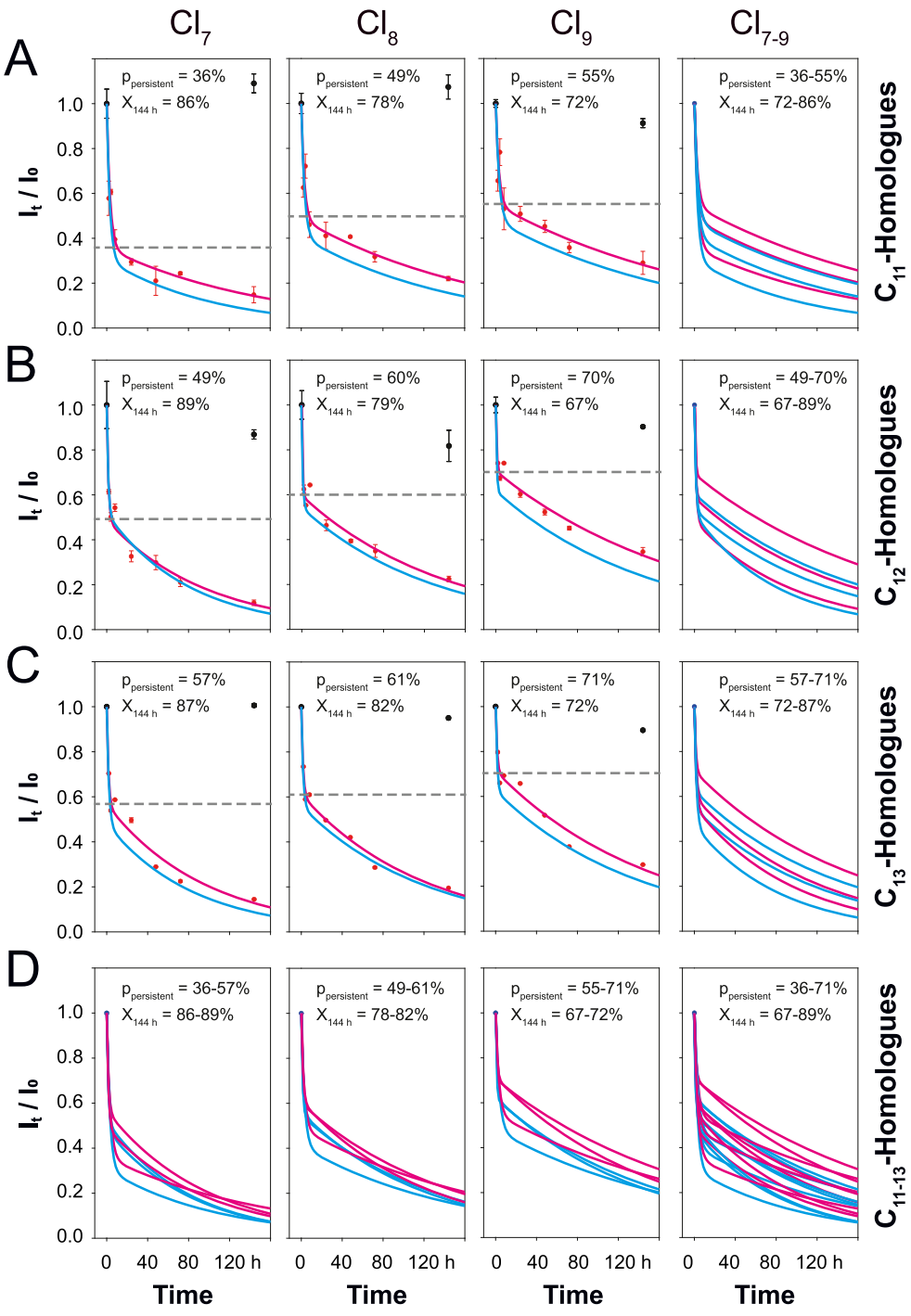

Fig. 6. Homologue-specific kinetic models for LinB-catalyzed transformations of COs (magenta) and CPs (blue). Relative intensities (I_t/I_0) of non-exposed (black, 0 h), LinB-exposed (magenta, 2–144 h) and buffer-exposed (control, black, 144 h) samples are depicted for Cl_7-, Cl_8-and Cl_9-undecenes (A), -dodecenes (B) and -tridecenes (C). Proportions (p_p) of persistent materials (dashed lines) and conversion efficiencies for respective CO-homologues are indicated. Overlaid diagrams compare kinetic models of CP- and CO-homologues with different chain-lengths and chlorination degrees (D). (For interpretation of the references to colour in this figure legend, the reader is referred to the Web version of this article.)

persistent material. The carbon-chain length (C_{11} to C_{13}) had a moderate influence on the proportions of persistent and reactive materials and no significant effect on the conversion efficiency. A significant effect of the chlorination degree on biotransformation was also found in another study (Fisk et al., 2000).

Table S13 shows kinetic constants from the bimodal first-order model for the fast early phase (k_{fast}) and slow latter phase (k_{slow}) of Cl_6-to Cl_{11}-chloro-undecanes, -dodecanes and -tridecanes. Kinetic constants of the reactive materials are 29–302 times larger than of persistent materials. For example, kinetic constants of Cl_6-to Cl_{10}-chloro-undecanes decrease steadily with the chlorination degree from $1.2{\cdot}10^{-2}$ to $5.0{\cdot}10^{-3}$ h^{-1} for persistent material and from 0.34 to 0.21 h^{-1} for reactive material (Table S13). From these kinetic parameters, half-lives were derived for both reactive ($\tau_{1/2,fast}$) and persistent ($\tau_{1/2,slow}$) homologues (Table S13). In general, half-lives of reactive materials were in order of hours (0.50–3.24 h) and the ones of persistent materials were in order of days (56–162 h). Thus, half-lives of persistent materials were two to three orders of magnitude lower than of reactive materials.

3.4. Comparison of LinB-catalyzed transformations of chlorinated olefins and paraffins

Fig. 6 compares measured (dots) and modeled (lines) conversion of hepta- (Cl_7), octa- (Cl_8) and nona- (Cl_9) chloro-olefins (magenta) and –paraffins (blue) of different chain lengths. Kinetic models of C_{11}- (A), C_{12}- (B) and C_{13}- (C) COs and CPs are shown together with overlays (D). LinB-catalyzed transformation of COs and CPs follow the same trend. As mentioned in chapter 3.2, LinB does not catalyze HCl-elimination reaction of CPs to COs. A substantial proportion of COs were converted quickly in the first 8 h. Afterwards (>8 h) CO conversion rates were much lower. In Table S16 kinetic parameters of CO transformations are reported, which were obtained accordingly with the two-phase first-

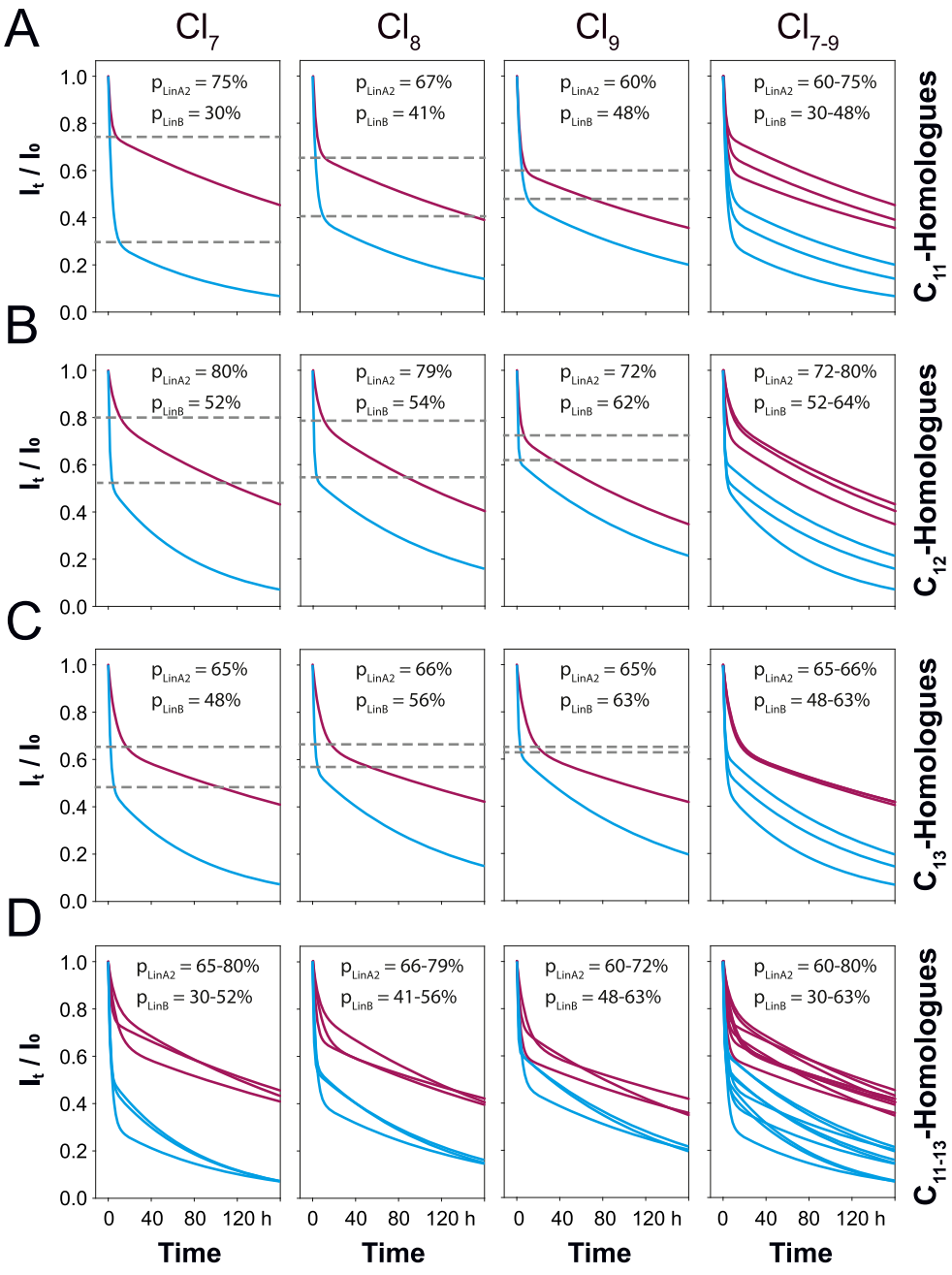

Fig. 7. Comparison of LinA2-and LinB-catalyzed transformations of different CP homologues. LinA2 data has been presented in another study (Heeb et al., 2019). Cl_7-, Cl_8-and Cl_9-undecanes (A), -dodecanes (B) and -tridecanes (C) are compared together with respective overlays (D). Bimodal first-order transformation kinetics can be observed for CPs exposed to LinA2 (magenta) and LinB (blue). Both, LinB- and LinA2-catalyzed transformations show a fast conversion of reactive material in an early phase and a slower conversion of persistent material in a latter phase. Proportions (p) of persistent CP material are indicated (gray lines) for LinA2 and LinB. In all cases, proportions of persistent material are higher for LinA2 conversion than for LinB. (For interpretation of the references to colour in this figure legend, the reader is referred to the Web version of this article.)

order kinetic model.

Conversion efficiencies of COs decreased with increasing chlorine number as those of CPs do (Fig. 5). Proportions of persistent COs also increased with chlorine number for all homologues like for CPs. The carbon-chain-length had only a small or no effect on the transformation efficiency.

As shown in Fig. 6, we observed slightly slower conversion rates of COs (magenta) than CPs (blue). In other words, CO model lines (magenta) do not cross those of CPs (blue). Half-lives ($\tau_{1/2}$) of reactive Cl_7-, Cl_8-and Cl_9-undecenes were 2.24, 1.98 and 2.10 h (Table S16). Those of respective undecanes were 2.09, 2.15 and 2.34 h, respectively (Table S13). Half-lives of persistent Cl_7-, Cl_8- and Cl_9-chlorinated undecenes were 110, 126 and 147 h, and those of respective chloroundecanes were 75, 105 and 128 h respectively (Tables S13 and S16). We conclude that reactive COs and CPs of individual homologues were converted by LinB in similar rates. But persistent CO materials were converted at 20–25% slower rates than respective CPs. Overall, this leads to lower conversion efficiencies of COs compared to CPs (Fig. 6).

3.5. Comparison of CP transformations kinetics of the bacterial enzymes LinA2 and LinB

In a previous *in-vitro* study, a similar bimodal kinetic was observed for the transformation of CPs with the dehalogenase LinA2 (Heeb et al., 2019). Both, LinA2-and LinB-enzymes are able to catalyze dechlorination reactions of CPs. Fig. 7 compares modeled conversion kinetics of LinB- (blue) and LinA2- (magenta) catalyzed transformation of Cl_7-, Cl_8-, Cl_9-undecanes (C_{11}, A), -dodecanes (C_{12}, B) and –tridecanes (C_{13}, C). Overlays of these data are also presented (Fig. 7). Similar substrates at identical concentrations were used in both studies, but enzymes and enzyme concentrations were different.

A LinB enzyme concentration of 3.0 μmol/L (100 mg/L) was used in this study. LinA2-concentration was 11.5 μmol/L (200 mg/L) in the previous study (Heeb et al., 2019). In other words, LinA2-concentration was almost 4-fold higher than the one of LinB. With this, one could expect a higher conversion of CPs with LinA2 than with LinB, assuming that both enzymes are equally efficient. However, specific activities of both enzymes were not evaluated in these studies. The activities might also have effects on the proportion of persistent material and amount of converted material.

As shown in Fig. 7, two-phase kinetics does apply in all cases, indicating that both enzymes show higher turnover rates for reactive and smaller rates for persistent material in CP-mixtures. Table S17 compares kinetic parameters for LinA2 and LinB. LinB showed a faster and more complete conversion of CPs than LinA2 did. As a general trend, we noticed that higher proportions of the material (60–80%) were persistent to LinA2. In comparison, proportions of only 36–71% were persistent with respect to LinB (Fig. 7). Lower-chlorinated CPs tend to contain more material that is persistent to LinA2 than higher-chlorinated CPs. The opposite trend was found for LinB, with less persistent material present in lower-chlorinated CPs.

However, the kinetic model is applicable for both enzymes. In both cases, some of the exposed CP material is reactive and some is persistent towards dehalogenation. Furthermore, the enzymatic transformation of CPs is more dependent on the chlorination degree than on the carbon chain-length. LinB preferentially catalyzes the transformations of CPs of lower-chlorinated materials. In contrast, LinA2 shows slightly higher conversion efficiencies for higher-chlorinated material.

4. Conclusions

The hexachlorocyclohexane-converting haloalkane dehalogenase LinB from *Spingobium Indicum* was able to convert chlorinated paraffins and olefins to hydroxylated transformation products *in-vitro*. All tested homologues of chlorinated paraffins, which included hexa- (Cl_6) to undeca-chloro-(Cl_{11}) undecanes (C_{11}), dodecanes (C_{12}) and tridecanes (C_{13}), were converted by LinB to some degree.

However, monitoring of dechlorination reactions of CPs in presence of COs is challenging due to strongly interfered mass spectra. The QTOF-MS used in this study was operated at a resolution of R ≈ 8′000. A resolution R > 30′000 is needed to resolve mass spectra of C_{11}-, C_{12}- and C_{13}-CPs from those of respective COs. Therefore, we had to process respective MS data and use a mathematical deconvolution procedure to distinguish paraffinic and olefinic material (Schinkel et al., 2018b; Knobloch et al., 2021). Background subtraction and subsequent deconvolution of respective isotope clusters improved the data quality. Non-interfered MS data could be deduced, which allowed to study homologue-specific transformation of CP and CO homologues.

Some of the exposed CP- and CO-material was converted within hours, some was transformed within days. Bimodal first-order kinetic models were applied to simulate homologue-specific dechlorination of CPs and COs. Conversion efficiencies varied substantially for homologues with different chlorination degree, whereas the carbon-chain length had only small effect. Proportions of persistent materials with varied as well for different homologues. Lower-chlorinated CPs and COs contained less persistent material than higher-chlorinated ones.

In conclusion, the bimodal first-order kinetic models allowed us to deduce homologue-specific reaction rates and proportions of reactive and persistent material. Furthermore, we could study effects of the chlorination degree and carbon-chain length on the persistence of CPs and COs towards LinB-catalyzed transformations. An relative enrichment of higher chlorinated CPs and COs in the remaining material indicates that the chlorination degree clearly affected LinB-catalyzed transformations.

We assume that longer-chain CPs, for example MCCPs and LCCPs, also contain both, reactive and persistent material and that the chlorination degree, more than the chain-length, may influence the persistence of MCCPs and LCCPs. Current legislation restricts CPs on the basis of the chain-length. It banned SCCPs and with it, expediated the use of MCCPs and LCCPs. We could show that shorter, lower-chlorinated CPs are transformed faster by LinB than longer, higher-chlorinated ones. In other words, longer higher-chlorinated CPs will likely accumulate in relative amounts in the remaining material. We assume that the conversion of higher-chlorinated MCCPs with LinB is also slower compared to the one of lower-chlorinated SCCPs. In this case, a substitution of SCCPs by longer-chained CPs is counterproductive.

Credit author statement

Marco Knobloch: Methodology, Validation, Software, Data curation, Supervision, Formal analysis, Investigation, Visualization, Writing – original draft, Writing – review & editing, Lena Schinkel: Methodology, Software, Writing – review & editing, Hans-Peter Kohler: Conceptualization, Resources, Supervision, Writing – review & editing, Flurin Mathis: Methodology, Investigation, Data curation, Software, Formal analysis, Visualization, Writing – review & editing, Susanne Kern: Supervision, Project administration, Resources, Methodology, Writing – review & editing, Davide Bleiner: Supervision, Project administration, Review, Norbert Heeb: Conceptualization, Methodology, Validation, Project administration, Funding acquisition, Resources, Supervision, Software, Formal analysis, Visualization, Writing – original draft, Writing – review & editing.

Funding

This work was supported by the Swiss Federal Office for the Environment (BAFU) (grant number: 19.0011.PJ/S113-1600).

Declaration of competing interest

The authors declare that they have no known competing financial interests or personal relationships that could have appeared to influence

the work reported in this paper.

Acknowledgement

We thank Thomas Fleischmann and Iris Schilling (Eawag) for their help and assistance in obtaining the LinB-enzyme.

Appendix A. Supplementary data

Supplementary data to this article can be found online at https://doi.org/10.1016/j.chemosphere.2021.131199.

References

Belkin, S., 1992. Biodegradation of haloalkanes. Biodegradation 3, 299–313. https://doi.org/10.1007/BF00129090.

Bergman, A., Hagman, A., Jacobsson, S., Jansson, B., Ahlman, M., 1984. Thermal degradation of polychlorinated alkanes. Chemosphere 13, 237–250. https://doi.org/10.1016/0045-6535(84)90130-9.

Chen, W., Yu, M., Zhang, Q., Hou, X., Kong, W., Wei, L., Mao, X., Liu, J., Schnoor, J., Jiang, G., 2020. Metabolism of SCCPs and MCCPs in suspension rice cells based on paired mass distance (PMD) analysis. Environ. Sci. Technol. https://doi.org/10.1021/acs.est.0c01830.

de Wit, C.A., Bossi, R., Dietz, R., Dreyer, A., Faxneld, S., Garbus, S.E., Hellström, P., Koschorreck, J., Lohmann, N., Roos, A., Sellström, U., Sonne, C., Treu, G., Vorkamp, K., Yuan, B., Eulaers, I., 2020. Organohalogen compounds of emerging concern in Baltic Sea biota: levels, biomagnification potential and comparisons with legacy contaminants. Environ. Int. 144, 106037. https://doi.org/10.1016/j.envint.2020.106037.

Diefenbacher, P.S., Bogdal, C., Gerecke, A.C., Glüge, J., Schmid, P., Scheringer, M., Hungerbühler, K., 2015. Short-chain chlorinated paraffins in zurich, Switzerland - atmospheric concentrations and emissions. Environ. Sci. Technol. 49, 9778–9786. https://doi.org/10.1021/acs.est.5b02153.

ECHA, 2019. Substance Evaluation Conclusion for Medium-Chain Chlorinated Paraffins/Alkanes, C14-17, Chloro. https://echa.europa.eu/de/information-on-chemicals/evaluation/community-rolling-action-plan/corap-table/-/dislist/details/0b0236e1807e3841.

Faber, K., 2018. Biotransformations in organic chemistry. Trends in Biotechnology. Springer International Publishing, Cham. https://doi.org/10.1007/978-3-319-61590-5.

Fiedler, H., 2010. Short-chain chlorinated paraffins: production, use and international regulations. The Handbook of Environmental Chemistry - Chlorinated Paraffins. Springer Nature, pp. 1–40. https://doi.org/10.1007/698.

Fisk, A.T., Tomy, G.T., Cymbalisty, C.D., Muir, D.C.G., 2000. Dietary accumulation and quantitative structure-activity relationships for depuration and biotransformation of short (C10), medium (C14), and long (C18) carbon-chain polychlorinated alkanes by juvenile rainbow trout (Oncorhynchus mykiss). Environ. Toxicol. Chem. 19, 1508–1516. https://doi.org/10.1002/etc.5620190606.

Glüge, J., Wang, Z., Bogdal, C., Scheringer, M., Hungerbühler, K., 2016. Global production, use, and emission volumes of short-chain chlorinated paraffins – a minimum scenario. Sci. Total Environ. 573, 1132–1146. https://doi.org/10.1016/j.scitotenv.2016.08.105.

He, C., van Mourik, L., Tang, S., Thai, P., Wang, X., Brandsma, S.H., Leonards, P.E.G., Thomas, K.V., Mueller, J.F., 2020. In vitro biotransformation and evaluation of potential transformation products of chlorinated paraffins by high resolution accurate mass spectrometry. J. Hazard Mater. 124245 https://doi.org/10.1016/j.jhazmat.2020.124245.

Heeb, N.V., Zindel, D., Geueke, B., Kohler, H.P.E., Lienemann, P., 2012. Biotransformation of hexabromocyclododecanes (HBCDs) with LinB - an HCH-converting bacterial enzyme. Environ. Sci. Technol. 46, 6566–6574. https://doi.org/10.1021/es2046487.

Heeb, N.V., Zindel, D., Graf, H., Azara, V., Bernd Schweizer, W., Geueke, B., Kohler, H.-P.E., Lienemann, P., 2013. Stereochemistry of LinB-catalyzed biotransformation of δ-HBCD to 1R,2R,5S,6R,9R,10S-pentabromocyclododecanol. Chemosphere 90, 1911–1919. https://doi.org/10.1016/j.chemosphere.2012.10.019.

Heeb, N.V., Schalles, S., Lehner, S., Schinkel, L., Schilling, I., Lienemann, P., Bogdal, C., Kohler, H.P.E., 2019. Biotransformation of short-chain chlorinated paraffins (SCCPs) with LinA2: a HCH and HBCD converting bacterial dehydrohalogenase. Chemosphere 226, 744–754. https://doi.org/10.1016/j.chemosphere.2019.03.169.

Heeb, N.V., Iten, S., Schinkel, L., Knobloch, M., Sprengel, J., Lienemann, P., Bleiner, D., Vetter, W., 2020. Characterization of synthetic single-chain CP standard materials – removal of interfering side products. Chemosphere 255, 126959. https://doi.org/10.1016/j.chemosphere.2020.126959.

Iozza, S., Schmid, P., Oehme, M., Bassan, R., Belis, C., Jakobi, G., Kirchner, M., Schramm, K.-W., Kräuchi, N., Moche, W., Offenthaler, I., Weiss, P., Simoncic, P., Knoth, W., 2009a. Altitude profiles of total chlorinated paraffins in humus and spruce needles from the Alps (MONARPOP). Environ. Pollut. 157, 3225–3231. https://doi.org/10.1016/j.envpol.2009.05.033.

Iozza, S., Schmid, P., Oehme, M., 2009b. Development of a comprehensive analytical method for the determination of chlorinated paraffins in spruce needles applied in passive air. sampling 157, 3218–3224. https://doi.org/10.1016/j.envpol.2009.06.033.

Knobloch, M.C., Schinkel, L., Schilling, I., Kohler, H.-P.E., Lienemann, P., Bleiner, D., Heeb, N.V., 2021. Transformation of short-chain chlorinated paraffins by the bacterial haloalkane dehalogenase LinB – formation of mono- and di-hydroxylated metabolites. Chemosphere 262, 128288. https://doi.org/10.1016/j.chemosphere.2020.128288.

Krätschmer, K., Schächtele, A., 2019. Interlaboratory studies on chlorinated paraffins: evaluation of different methods for food matrices. Chemosphere 234, 252–259. https://doi.org/10.1016/j.chemosphere.2019.06.022.

Labadie, P., Blasi, C., Le Menach, K., Geneste, E., Babut, M., Perceval, O., Budzinski, H., 2019. Evidence for the widespread occurrence of short- and medium-chain chlorinated paraffins in fish collected from the Rhône River basin (France). Chemosphere 223, 232–239. https://doi.org/10.1016/j.chemosphere.2019.02.069.

Lal, R., Saxena, D.M., 1982. Accumulation, metabolism and effects of organochlorine insecticides on microorganisms. Microbiol. Rev. 46, 95–127. https://doi.org/10.1128/mmbr.46.1.95-127.1982.

Lal, R., Pandey, G., Sharma, P., Kumari, K., Malhotra, S., Pandey, R., Raina, V., Kohler, H.-P.E., Holliger, C., Jackson, C., Oakeshott, J.G., 2010. Biochemistry of microbial degradation of hexachlorocyclohexane and prospects for bioremediation. Microbiol. Mol. Biol. Rev. 74, 58–80. https://doi.org/10.1128/MMBR.00029-09.

Li, Y., Hou, X., Chen, W., Liu, J., Zhou, Q., Schnoor, J.L., Jiang, G., 2019. Carbon chain decomposition of short chain chlorinated paraffins (SCCPs) mediated by pumpkin and soybean seedlings. Environ. Sci. Technol. 53, 6765–6772. https://doi.org/10.1021/acs.est.9b01215.

Liu, R., Zhang, C., Kang, L., Sun, X., Zhao, Y., 2015. The OH-initiated chemical transformation of 1,2,4,6,8,10,11-heptachloroundecane in the atmosphere. RSC Adv. 5, 37988–37994. https://doi.org/10.1039/C5RA00612K.

Loos, M., Gerber, C., Corona, F., Hollender, J., Singer, H., 2015. Accelerated isotope fine structure calculation using pruned transition trees. Anal. Chem. 87, 5738–5744. https://doi.org/10.1021/acs.analchem.5b00941.

Matsukami, H., Takemori, H., Takasuga, T., Kuramochi, H., Kajiwara, N., 2020. Liquid chromatography–electrospray ionization-tandem mass spectrometry for the determination of short-chain chlorinated paraffins in mixed plastic wastes. Chemosphere 244, 125531. https://doi.org/10.1016/j.chemosphere.2019.125531.

Mézière, M., Cariou, R., Larvor, F., Bichon, E., Guitton, Y., Marchand, P., Dervilly, G., Bruno, L.B., 2020. Optimized characterization of short-, medium, and long-chain chlorinated paraffins in liquid chromatography-high resolution mass spectrometry. J. Chromatogr. A 1619, 460927. https://doi.org/10.1016/j.chroma.2020.460927.

Muir, D.C.G., Stern, G.A., Tomy, G.T., 2000. Chlorinated paraffins. The Handbook of Environmental Chemistry - Anthropogenic Compounds. Springer-Verlag, Berlin Heidelberg, pp. 203–236.

Nagata, Y., Miyauchi, K., Takagi, M., 1999. Complete analysis of genes and enzymes for γ-hexachlorocyclohexane degradation in Sphingomonas paucimobilis UT26. J. Ind. Microbiol. Biotechnol. 23, 380–390. https://doi.org/10.1038/sj.jim.2900736.

Perkons, I., Pasecnaja, E., Zacs, D., 2019. The impact of baking on chlorinated paraffins: characterization of C10–C17 chlorinated paraffins in oven-baked pastry products and unprocessed pastry dough by HPLC–ESI–Q–TOF–MS. Food Chem. 298, 125100. https://doi.org/10.1016/j.foodchem.2019.125100.

Schinkel, L., Lehner, S., Heeb, N.V., Lienemann, P., McNeill, K., Bogdal, C., 2017. Deconvolution of mass spectral interferences of chlorinated alkanes and their thermal degradation products: chlorinated alkenes. Anal. Chem. 89, 5923–5931. https://doi.org/10.1021/acs.analchem.7b00331.

Schinkel, L., Lehner, S., Heeb, N.V., Marchand, P., Cariou, R., McNeill, K., Bogdal, C., 2018a. Dealing with strong mass interferences of chlorinated paraffins and their transformation products: an analytical guide. TrAC Trends Anal. Chem. (Reference Ed.) 106, 116–124. https://doi.org/10.1016/j.trac.2018.07.002.

Schinkel, L., Lehner, S., Knobloch, M., Lienemann, P., Bogdal, C., McNeill, K., Heeb, N.V., 2018b. Transformation of chlorinated paraffins to olefins during metal work and thermal exposure – deconvolution of mass spectra and kinetics. Chemosphere 194, 803–811. https://doi.org/10.1016/j.chemosphere.2017.11.168.

Sprengel, J., Wiedmaier-Czerny, N., Vetter, W., 2019. Characterization of single chain length chlorinated paraffin mixtures with nuclear magnetic resonance spectroscopy (NMR). Chemosphere 228, 762–768. https://doi.org/10.1016/j.chemosphere.2019.04.094.

Sprengel, J., Vetter, W., 2020. NMR and GC/MS analysis of industrial chloroparaffin mixtures. Anal. Bioanal. Chem. 412, 4669–4679. https://doi.org/10.1007/s00216-020-02720-7.

Tomy, G.T., 2010. Analysis of Chlorinated Paraffins in Environmental Matrices: the Ultimate Challenge for the Analytical Chemist, pp. 83–106. https://doi.org/10.1007/698_2009_39.

UNEP, 2012. Short-chained chlorinated paraffins - revised draft risk profile (UNEP/POPS/POPRC.8/6). Persistent Org. Pollut. Rev. Comm.

UNEP, 2016. Report of the Persistent Organic Pollutants Review Committee on the Work of its Twelfth Meeting. UNEP/POPS/POPRC.12/11/Add.3 1–36.

UNEP, 2017. Decision SC-8/11 : Listing of Short-Chain Chlorinated Paraffins 14.

van Mourik, L.M., Gaus, C., Leonards, P.E.G., de Boer, J., 2016. Chlorinated paraffins in the environment: a review on their production, fate, levels and trends between 2010 and 2015. Chemosphere 155, 415–428. https://doi.org/10.1016/j.chemosphere.2016.04.037.

van Mourik, L.M., van der Veen, I., Crum, S., de Boer, J., 2018. Developments and interlaboratory study of the analysis of short-chain chlorinated paraffins. TrAC Trends Anal. Chem. (Reference Ed.) 102, 32–40. https://doi.org/10.1016/j.trac.2018.01.004.

Vogel, T.M., Criddle, C.S., McCarty, P.L., Arcos, J.C., 1987. Transformations of halogenated aliphatic compounds: oxidation, reduction, substitution, and dehydrohalogenation reactions occur abiotically or in microbial and mammalian

systems. Environ. Sci. Technol. 21, 722–736. https://doi.org/10.1021/es00162a001.

Vorkamp, K., Rigét, F.F., 2014. A review of new and current-use contaminants in the Arctic environment: evidence of long-range transport and indications of bioaccumulation. Chemosphere 111, 379–395. https://doi.org/10.1016/j.chemosphere.2014.04.019.

Wang, X., Zhu, J., Xue, Z., Jin, X., Jin, Y., Fu, Z., 2019. The environmental distribution and toxicity of short-chain chlorinated paraffins and underlying mechanisms: implications for further toxicological investigation. Sci. Total Environ. 695, 133834. https://doi.org/10.1016/j.scitotenv.2019.133834.

Yuan, B., Alsberg, T., Bogdal, C., MacLeod, M., Berger, U., Gao, W., Wang, Y., De Wit, C. A., 2016. Deconvolution of soft ionization mass spectra of chlorinated paraffins to resolve congener groups. Anal. Chem. 88, 8980–8988. https://doi.org/10.1021/acs.analchem.6b01172.

Yuan, B., Lysak, D.H., Soong, R., Haddad, A., Hisatsune, A., Moser, A., Golotvin, S., Argyropoulos, D., Simpson, A.J., Muir, D.C.G., 2020. Predicted NMR Pattern Matching Framework for Isomeric. https://doi.org/10.1021/acs.estlett.0c00244.